ACS APPLIED MATERIALS & INTERFACES

Research Article

www.acsami.org

Integrated Logic Gate for Fluorescence Turn-on Detection of Histidine and Cysteine Based on Ag/Au Bimetallic Nanoclusters−Cu^{2+} Ensemble

Jian Sun,[†] Fan Yang,[†] Dan Zhao,[†,‡] Chuanxia Chen,[†,‡] and Xiurong Yang*,[†]

[†]State Key Laboratory of Electroanalytical Chemistry, Changchun Institute of Applied Chemistry, Chinese Academy of Sciences, Changchun, Jilin 130022, China

[‡]University of Chinese Academy of Sciences, Beijing 100039, China

Supporting Information

ABSTRACT: By means of employing 11-mercaptoundecanoic acid (11-MUA) as a reducing agent and protecting ligand, we present straightforward one-pot preparation of fluorescent Ag/Au bimetallic nanoclusters (namely AgAuNCs@11-MUA) from $AgNO_3$ and $HAuCl_4$ in alkaline aqueous solution at room temperature. It is found that the fluorescence of AgAuNCs@11-MUA has been selectively quenched by Cu^{2+} ions, and the nonfluorescence off-state of the as-prepared AgAuNCs@11-MUA−Cu^{2+} ensemble can be effectively switched on upon the addition of histidine and cysteine. By incorporating Ni^{2+} ions and N-ethylmaleimide, this phenomenon is further exploited as an integrated logic gate and a specific fluorescence turn-on assay for selectively and sensitively sensing histidine and cysteine has been designed and established based on the original noncovalent AgAuNCs@11-MUA−Cu^{2+} ensemble. Under the optimal conditions, histidine and cysteine can be detected in the concentration ranges of 0.25−9 and 0.25−7 μM; besides, the detection limits are found to be 87 and 111 nM (S/N = 3), respectively. Furthermore, we demonstrate that the proposed AgAuNCs@11-MUA-based fluorescent assay can be successfully utilized for biological fluids sample analysis.

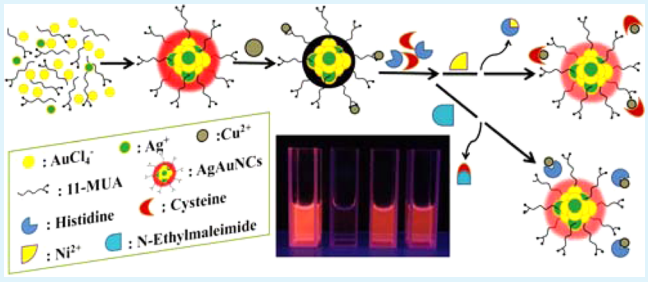

KEYWORDS: *Ag/Au bimetallic nanoclusters, integrated logic gate, fluorescence turn-on, histidine, cysteine, 11-mercaptoundecanoic acid*

INTRODUCTION

Owing to their intrinsic high sensitivity and spatiotemporal resolution, fluorescent sensors are undoubtedly one of the most efficient and accessible devices that have been used in biologically relevant molecular recognition[1−3] and biomedical diagnosis.[4,5] Thereinto, choosing correct fluorescent materials and transformation of the sensing events into changes in the fluorescent signal are two key issues for fluorescent sensing. Over the past few decades, highly fluorescent noble metal nanoclusters (NCs, typically Au and Ag) have attracted significant attention as one candidate of the most promising fluorescent sensors, due to their ultrasmall size, good biocompatibility, and obvious intrinsic fluorescence.[6−8] Relative to Au nanoclusters (AuNCs), Ag nanoclusters (AgNCs) usually have lower photo- and thermo-stability, but greater quantum yields.[9−11] Recently, several fluorescent Ag/Au bimetallic NCs (AgAuNCs) with superior chemical and physical properties have been prepared and the introduction of Ag into the AuNCs could produce significant fluorescent enhancement.[12−14] These advances in the synthetic process and emission mechanism of AgAuNCs shall benefit for the development of more sensitive sensing techniques. Simultaneously, among the different types of protecting agents, thiolate ligands are the most commonly adopted candidates for noble metals NCs due to their readily modification, potential selective recognition function and extraordinary stability of the resultant NCs, which are beneficial to the fabrication of NC-based fluorescent sensors.[8,15,16] Thus, by ingenious integration of a suitable receptor binding group into the thiolate molecules, metal ions sensors for Hg^{2+}, Cr^{3+}, Cu^{2+}, and Ag^+ have been well developed based on the propensity to quench the fluorescence of thiolate-NCs.[6−8,17−21] Prompted by several organic molecules/metal ions complex-based fluorescence turn-on assays,[22,23] the noncovalent NCs@ligands−metal ions ensembles have also been proposed and applied in a competitive sensing system,[24−26] where the target analytes readily recover the fluorescence by selectively snatching the metal ions from NCs because of the higher coordination reactivity between analytes and metal ions than that between NCs@ligands and metal ions.

Being the naturally occurring amino acids, both histidine (His) and cysteine (Cys) play critical roles in human lives and many critical bioactivities.[1] For instance, His is an important neurotransmitter and its metabolism disorder is an indicator for psychological disorders and many diseases.[27,28] Similarly, the

Received: January 15, 2015
Accepted: March 12, 2015
Published: March 12, 2015

DOI: 10.1021/acsami.5b00434
ACS Appl. Mater. Interfaces 2015, 7, 6860−6866

Scheme 1. Schematic Representation of the Synthetic Strategy for AgAuNCs@11-MUA Preparation and Amino Acids Sensing Mechanism

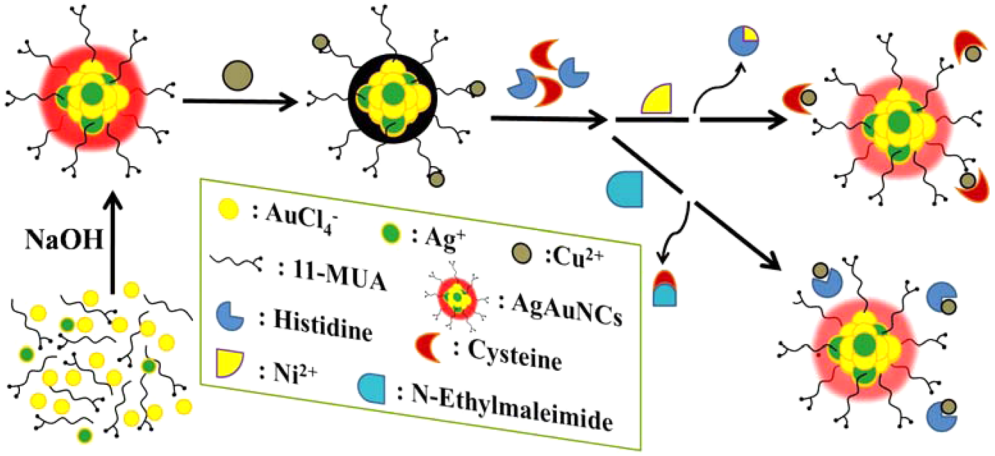

deficiency of Cys in the human body[29] results in hair depigmentation, skin lesions, edema, lethargy, liver damage, and loss of muscle and fat, whereas an elevated Cys level is known to result in cardiovascular and Alzheimer's diseases.[30,31] Besides being present at the active site of several metalloenzymes, His and Cys often act as powerful detoxifiers and regulators of metal transmission in biological fluids due to their high binding affinity toward several metal ions.[32,33] Inspired by this potential preferential interaction between His/Cys and metal ions, in connection with the reversible fluorescent change of the noncovalent NCs@ligands−metal ions ensembles, we herein describe our proposal for a AgAuNCs-based sensing ensemble, which is amenable to selective detection of His and Cys, respectively. In brief, we first present one-pot synthesis of fluorescent AgAuNCs capped with 11-MUA (namely AgAuNCs@11-MUA) from $AgNO_3$ and $HAuCl_4$ by simply utilizing 11-MUA as a reducing agent and protecting ligand in alkaline aqueous solution (Scheme 1). Subsequently, the fluorescence of AgAuNCs@11-MUA would be quenched upon the addition of Cu^{2+} ion, and the fluorescence of the as-prepared AgAuNCs@11-MUA−Cu^{2+} ensemble would be restored in the presence of His or Cys (Figure S1 in the Supporting Information). With the separate introduction of Ni^{2+} ions or N-ethylmaleimide (NEM), which showed a corresponding recognized masking effect for His[34] or Cys,[35] respectively, the aforementioned ensemble has been constructed as an integrated logic gate for not only fluorescence turn-on detection but also differentiation of His and Cys (Scheme 1).

EXPERIMENTAL SECTION

Reagents and Materials. Silver nitrate ($AgNO_3$), hydrogen tetrachloroaurate trihydrate ($HAuCl_4{\cdot}3H_2O$), copper(II) sulfate pentahydrate ($CuSO_4{\cdot}5H_2O$), 11-mercaptoundecanoic acid (11-MUA), and N-ethylmaleimide (NEM) were purchased from Sigma-Aldrich (St. Louis, MO, USA). Sodium hydroxide (NaOH) and 4-(2-hydroxyethyl)-1-piperazineethanesulfonic acid (HEPES) were purchased from Aladdin Industrial Corporation (Shanghai, China). NaCl, KCl, $CaCl_2$, $MgCl_2$, $MnCl_2$, $FeCl_3$, $CoCl_2$, $NiCl_2$, $Zn(NO_3)_2$, $PbCl_2$, $CdCl_2$, and $HgCl_2$ were purchased from Beijing Chemical Works. Histidine, cysteine, and other essential amino acids for the human beings were purchased from DingGuo Biotech. Ltd. (Beijing, China) and Sigma-Aldrich (St. Louis, MO, USA), respectively. All chemicals used were of analytical grade at least. For all aqueous solutions, the ultrapure water from a Millipore system was used.

Characterizations. Transmission electron microscopy (TEM) and high resolution TEM (HRTEM) measurements were carried out by using a FEI TECNAI F20 EM with an accelerating voltage of 200 kV equipped with an energy dispersive spectrometer. The X-ray photoelectron spectroscopy (XPS) measurements were performed with Thermo ESCALAB VG Scientific 250 and equipped with monochromatized Al Kα excitation. UV−vis absorption spectra were recorded by a CARY 500 UV−vis-NIR Varian spectrophotometer using a 1 cm path length quartz cell at room temperature. The fluorescence intensity (FL) measurements were performed on a Hitachi F-4600 spectrofluorometer (Tokyo, Japan). Inductively coupled plasma optical emission spectrometry (ICP-OES) analysis was conducted with an iCAP 6300 of Thermo scientific instrument. Photostability tests were performed by using our previously reported strategy.[24]

Preparation and Purification of AgAuNCs@11-MUA and AuNCs@11-MUA. The Ag/Au bimetallic nanoclusters capped with 11-MUA (AgAuNCs@11-MUA) were synthesized according to a modified one-pot strategy that we used to prepare AuNCs.[18] Typically, 11-MUA (26.2 mg) and NaOH (0.3 mL, 1 M) were completely dissolved in 16.7 mL of water, followed by rapid addition of the solution of $HAuCl_4$ (2.4 mL, 10 mM) and $AgNO_3$ (0.6 mL, 10 mM) at room temperature. Immediately, the thorough mixture exhibited the red fluorescence, visible to the naked eye, under ultraviolet light, and was then left to stand for 5 h at room temperature under no stirring, where the solution remained colorless. The solution after synthesis was taken into 8−14 kDa cutoff dialysis bag and dialyzed against ultrapure water for more than 24 h with four changes, to remove all impurities. The as-obtained purified AgAuNCs@11-MUA aqueous solution was stored at 4 °C for further use. The element concentrations of the as-obtained AgAuNCs were determined by ICP-OES, and we defined the total concentration of metal (Ag and Au) as the concentration of the AgAuNCs@11-MUA.

The preparation and purification of the monometallic Au NCs capped with 11-MUA (AuNCs@11-MUA) are based on that of AgAuNCs@11-MUA by just adding $HAuCl_4$ (3.0 mL, 10 mM) instead of the addition of a solution of $HAuCl_4$ (2.4 mL, 10 mM) and $AgNO_3$ (0.6 mL, 10 mM).[18]

Detection Procedures. To evaluate the effect of Cu^{2+} ions on the fluorescence quenching of AgAuNCs@11-MUA, 0.5 mL of 20 μM AgAuNCs@11-MUA aqueous solution, 1.0 mL of 20 mM 4-(2-hydroxyethyl)-1-piperazineethanesulfonic acid (HEPES) buffer (pH 7.4) and different amounts of Cu^{2+} were sequentially added to a 2 mL calibrated test tube. The mixture was diluted to volume (2.0 mL) with ultrapure water, shaken drastically, and equilibrated for 10 min to measure the fluorescence emission spectra.

To detect histidine, 0.5 mL of 20 μM AgAuNCs@11-MUA aqueous solution, 1.0 mL of 20 mM HEPES buffer (pH 7.4), 4 μL of 1 mM Cu^{2+} solution, and 0.2 mL of 1 mM NEM were sequentially added to a

DOI: 10.1021/acsami.5b00434
ACS Appl. Mater. Interfaces 2015, 7, 6860−6866

2 mL calibrated test tube. The mixture was shaken thoroughly and equilibrated for 10 min. The 10 μL of different concentration of histidine standard solution and 286 μL of ultrapure water were then added, and the mixture was further shaken drastically, and equilibrated for 1 min to measure the fluorescence emission spectra.

To detect cysteine, 0.5 mL of 20 μM AgAuNCs@11-MUA aqueous solution, 1.0 mL of 20 mM HEPES buffer (pH 7.4), 4 μL of 1 mM Cu^{2+} solution, and 20 μL of 1 mM Ni^{2+} were sequentially added to a 2 mL calibrated test tube. The mixture was shaken thoroughly and equilibrated for 10 min. The 10 μL of different concentration of cysteine standard solution and 466 μL of ultrapure water were then added, and the mixture was further shaken thoroughly, and equilibrated for 1 min to measure the fluorescence emission spectra.

To evaluate the detection selectivity, other essential amino acids for the human beings such as alanine, arginine, aspartic acid, asparagine, glutamine, glutamic acid, glycine, isoleucine, leucine, lysine, methionine, phenylalanine, proline, serine, threonine, tryptophan, tyrosine, and valine were individually investigated and measured.

Detection of Histidine in Human Urine. Human urine samples were collected from healthy volunteers and needed no other pretreatments except being diluted with ultrapure water. To detect histidine in diluted urine samples, 0.5 mL of 20 μM AgAuNCs@11-MUA aqueous solution, 1.0 mL of 20 mM HEPES buffer (pH 7.4), 4 μL of 1 mM Cu^{2+} solution, and 0.2 mL of 1 mM NEM were sequentially added to a 2 mL calibrated test tube. The mixture was shaken drastically and equilibrated for 10 min. The 100 μL of different concentration of histidine standard solution, 100 μL of different concentrations of the diluted urine samples, and 96 μL of ultrapure water were then added, and the mixture was further shaken thoroughly, and equilibrated for 1 min to measure the fluorescence emission spectra.

RESULTS AND DISCUSSION

Through the direct coreduction of $AgNO_3$ and $HAuCl_4$ in alkaline aqueous solution at room temperature, we have easily acquired the AgAuNCs@11-MUA, which appears nearly colorless and bright red fluorescence in the presence of visible and ultraviolet light, respectively (the inset of Figure 1A). In contrast to the monometallic AuNCs@11-MUA, it possesses the similar absorption spectrum, but obvious bathochromic shifts of fluorescence emission and excitation peaks (320 and 630 nm for AgAuNCs vs 280 and 610 nm for AuNCs) (Figure 1A and Figure S2 in the Supporting Information). Using Rhodamine B (quantum yield = 31% in water) as the reference, the quantum yields of our as-prepared fluorescent nanoclusters in aqueous solution were determined as ~4.2% for AgAuNCs@11-MUA and ~2.4% for AuNCs@11-MUA. The results illustrated that the introduction of silver allowed a fluorescence enhancement compared to the recent AuNCs@11-MUA. In addition, as shown in Figure S3 in the Supporting Information, the fluorescence intensity of AgAuNCs@11-MUA only decreased <20% under ultraviolet light irradiation for 2 h, which indicated its good photostability and did not differ significantly from the case of AuNCs@11-MUA.

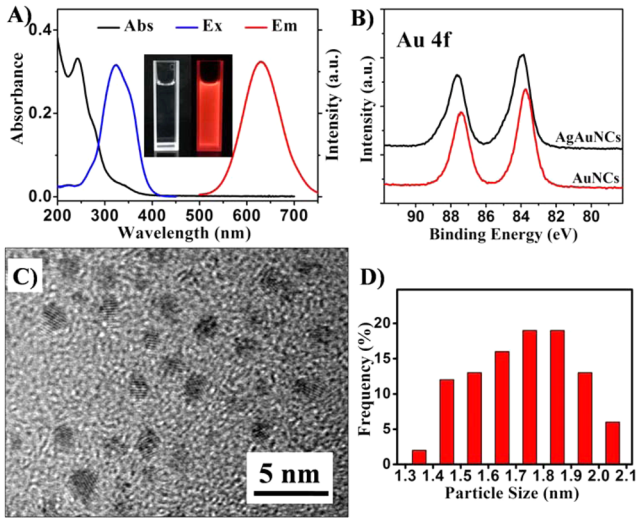

Figure 1. (A) UV–vis absorption (black), FL excitation (blue), and emission (red) spectra of AgAuNCs@11-MUA. The inset shows the photographs of AgAuNCs under the visible (left) and ultraviolet light (right). (B) XPS spectra of Au 4f for AgAuNCs (black) and AuNCs (red). (C) HRTEM image of the AgAuNCs@11-MUA. (D) Size distribution of the AgAuNCs@11-MUA in diameter.

The XPS of the as-prepared fluorescent nanoclusters shows that a higher binding energy of Au $4f_{7/2}$ of the AgAuNCs (~84.0 eV) was observed compared to that of AuNCs (~83.7 eV) (Figure 1B). It is illustrated that a higher percentage of Au^+ exists in the resultant bimetallic AgAuNCs, compared to that in the monometallic AuNCs.[36,37] Simultaneously, the XPS spectra of Ag 3d and S 2p (Figure S4 in the Supporting Information) have confirmed the domination of Ag in its zero valence form and 11-MUA as the protecting ligand in the resultant AgAuNCs. In addition, transmission electron microscopy (TEM) (Figure S5A in the Supporting Information) and high resolution TEM (HRTEM) (Figure 1C) were used to evaluate the size distribution and morphology of AgAuNCs@11-MUA, which revealed an average diameter of 1.71 ± 0.19 nm, roughly spherical and well monodisperse for the AgAuNCs (Figure 1D). Furthermore, we have used ICP-OES in the determination of gold, silver, and sulfur elements in the resultant AgAuNCs@11-MUA and the calculated molar ratio of Ag-to-Au (1:4.1) is close to the ratio of the initial $AgNO_3$ and $HAuCl_4$ (1:4) (Table S1 in the Supporting Information). The elemental compositions of the AgAuNCs were also qualitatively confirmed from the EDX spectra (Figure S6 in the Supporting Information). All of these experimental results have demonstrated that AgAuNCs@11-MUA with superior performance can be easily prepared by a direct one-pot synthetic approach.

To construct the sensing ensemble at a nonfluorescence off-state and investigate the interference of other metal ions to potential detection, a variety of metal ions (Na^+, K^+, Ca^{2+}, Mg^{2+}, Mn^{2+}, Fe^{3+}, Co^{2+}, Ni^{2+}, Cu^{2+}, Zn^{2+}, Ag^+, Pb^{2+}, Hg^{2+}, and Cd^{2+}) were systematically introduced into the pH 7.4 HEPES buffer of AgAuNCs@11-MUA (5 μM). Upon treatment with different metals, the fluorescence of AgAuNCs was found to be unambiguously quenched just by Cu^{2+}, while a slight decrease in fluorescence was induced by Co^{2+} and Ni^{2+} (Figure 2A). The selective interaction between AgAuNCs and Cu^{2+} had been further investigated. As indicated in Figure 3, the addition of Cu^{2+} into the AgAuNCs solution resulted in that the fluorescence intensity of 11-MUA-AuNPs was quenched gradually with the increasing concentration of Cu^{2+} (0.1–5 μM). It was substantiated that 2 μM of Cu^{2+} could induce ~90% quenching of the initial fluorescence intensity, and this concentration of 2 μM for Cu^{2+} would be employed to construct the following sensing ensemble.

Subsequently, the as-prepared AgAuNCs@11-MUA–Cu^{2+} ensemble in buffer was treated respectively with twenty essential amino acids, and the fluorescence intensity ratios of sensing ensemble in the absence and presence of 10 μM various amino acids were recorded. As shown in Figure 2B, both His and Cys could recover the fluorescence of Cu^{2+}-quenched

DOI: 10.1021/acsami.5b00434
ACS Appl. Mater. Interfaces 2015, 7, 6860–6866

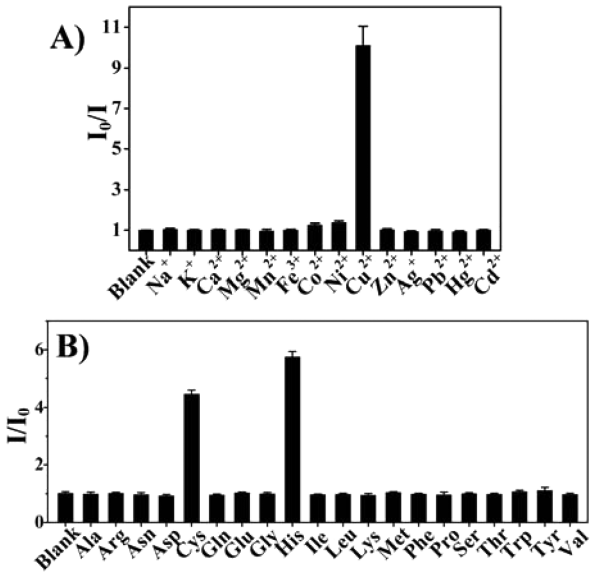

Figure 2. (A) FL intensity ratios (I_0/I at 630 nm, where I_0 and I are the FL intensities in the absence and presence of the analytes, respectively) for the AgAuNCs (5 μM) measured after the addition of 2 μM various individual metal ions in 10 mM HEPES buffer at pH 7.4. (B) FL intensity ratios (I/I_0 at 630 nm) for the AgAuNCs@11-MUA–Cu^{2+} ensemble measured after the addition of 10 μM various individual amino acids in pH 7.4, 10 mM HEPES buffer.

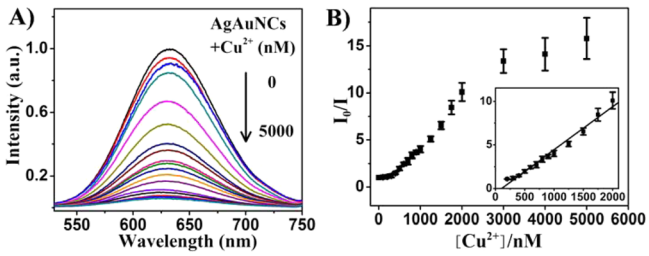

Figure 3. (A) FL emission spectra of the AgAuNCs@11-MUA in the presence of different Cu^{2+} ions concentrations (top to bottom, 0–5 μM). (B) Relative fluorescence intensities (I_0/I at 630 nm) for AgAuNCs vs the Cu^{2+} concentrations. Inset: plots of I_0/I against the Cu^{2+} ions concentrations. Measurements were performed by using 5 μM AgAuNCs in pH 7.4, 10 mM HEPES buffer.

AgAuNCs, but other amino acids did not induce significant change in the fluorescence emission intensity. In the control experiment, the fluorescence of the sole AgAuNCs@11-MUA without Cu^{2+} in HEPES buffer exhibited a nearly negligible alteration in the presence of twenty various essential amino acids (Figure S7 in the Supporting Information).

Due to its intrinsic paramagnetic properties and high coordination ability to special organic groups (such as carboxyl, amine, and thiol groups), Cu^{2+} has the tendency to reduce the fluorescence of several fluorescent materials through proper binding sites and a series of related assay systems have recently been developed.[23−25] Likewise, the Cu^{2+}–induced quenching mechanism of AgAuNCs@11-MUA in this report should be referred to the coordination of Cu^{2+} with the carboxyl group of 11-MUA, as well as the subsequent formation of the AuNCs@11-MUA–Cu^{2+} ensemble.[24] Several previous reports have elucidated that the interaction between His/Cys and Cu^{2+} has higher coordination reactivity compared to the affinity between the sole carboxyl group and Cu^{2+}.[33,38,39] Therefore, it is not surprising that the nonfluorescence off-state of the AuNCs@11-MUA–Cu^{2+} ensemble would be effectively switched on by the addition of His or Cys due to the seizure and snatching of Cu^{2+} from the ensemble by His/Cys. This sensing mechanism has also been confirmed from the further TEM experiments (Figure S5 in the Supporting Information). Taking Cys as an example, upon the sequential addition of Cu^{2+} and Cys, the typical TEM images and corresponding size distribution histograms of the AgAuNCs@11-MUA solution showed negligible change, which implied that the reversible competitive coordination of Cu^{2+} between AgAuNCs@11-MUA and Cys could be drawn into the fluorescence quenching and restoring process. The case of the addition of His had a similar phenomenon, and the data are not shown here.

To further improve the detection selectivity and differentiate His and Cys, we added a common Cys scavenger, NEM, for eliminating the interference of Cys, and a recognized His-binding metal ions, Ni^{2+}, for shielding His in the AgAuNCs@11-MUA–Cu^{2+} ensemble-based assay. As NEM selectively masked Cys, we were able to quantitatively evaluate the His by using the sensing ensemble, whereas an opposite result was found in the presence of Ni^{2+}. This phenomenon for chemically driven molecular switches, which can be converted from one fluorescent state into another by an external additive stimulus, can be described and manipulated as molecular logic gates.[40,41] As shown in Figure 4, the AgAuNCs–Cu^{2+} ensemble-based integrated logic gates exhibit fluorescence emission as the optical output in response to four inputs: Cys, His, Ni^{2+}, and NEM. In the case of no input, the relative fluorescence intensity (I/I_0 at 630 nm) of AgAuNCs–Cu^{2+} ensemble relative to the initial AgAuNCs remained only about 0.1. However, if either Cys or His was the input, the relative intensity increased to more than 0.5. In addition, after NEM or Ni^{2+} shielding the Cys or His, separately, there was precious little free Cys or His to snatch the Cu^{2+} and no obvious fluorescence recovery as the output. The output ratio below and above the threshold value of 0.3 defined as "0" and "1", respectively. Considering the 16 input modes, with each input mode corresponding to a result, the fluorescent experimental results are shown in Figure 4B,C. The truth table shows the results of each input mode in Figure 4D, and the logic scheme of the integrated logic gate composed of two INHIBIT gates and one OR gate is described in Figure 4E. The His/Cys concentration-dependent fluorescence enhancement has been quantitatively investigated by using the AgAuNCs@11-MUA–Cu^{2+} ensemble as the amino acids sensor. As indicated in Figure 5A, a continuous increase in the fluorescence of the AgAuNCs@11-MUA–Cu^{2+} ensemble was observed with the gradual addition of His (0.25–50 μM) in the presence of 100 μM NEM.

Along with the His concentrations increasing from 0.25 to 9 μM, the intensity ratios (I/I_0 at 630 nm, where I_0 and I are the corresponding fluorescence intensities in the absence and presence of His, respectively) displayed a quasilinear relationship (the inset of Figure 5B). The regression equation could be described as $I/I_0 = 1 + 0.442$ [His] ($R^2 = 0.995$). Under the current experimental conditions, the detection limit of His was estimated to be 87 nM, at a signal-to-noise ratio of 3. Likewise, a continuous increase in the fluorescence of the AgAuNCs@11-MUA–Cu^{2+} ensemble was achieved with the gradual addition of Cys (0.25–50 μM) in the presence of 10 μM Ni^{2+}, and the intensity ratios I/I_0 showed a quasilinear relationship with the Cys concentration within the range of 0.25 to 7 μM (Figure 5C,D). The regression equation could be described as $I/I_0 = 1 + 0.347$ [Cys] ($R^2 = 0.992$), and the detection limit of Cys was

DOI: 10.1021/acsami.5b00434
ACS Appl. Mater. Interfaces 2015, 7, 6860−6866

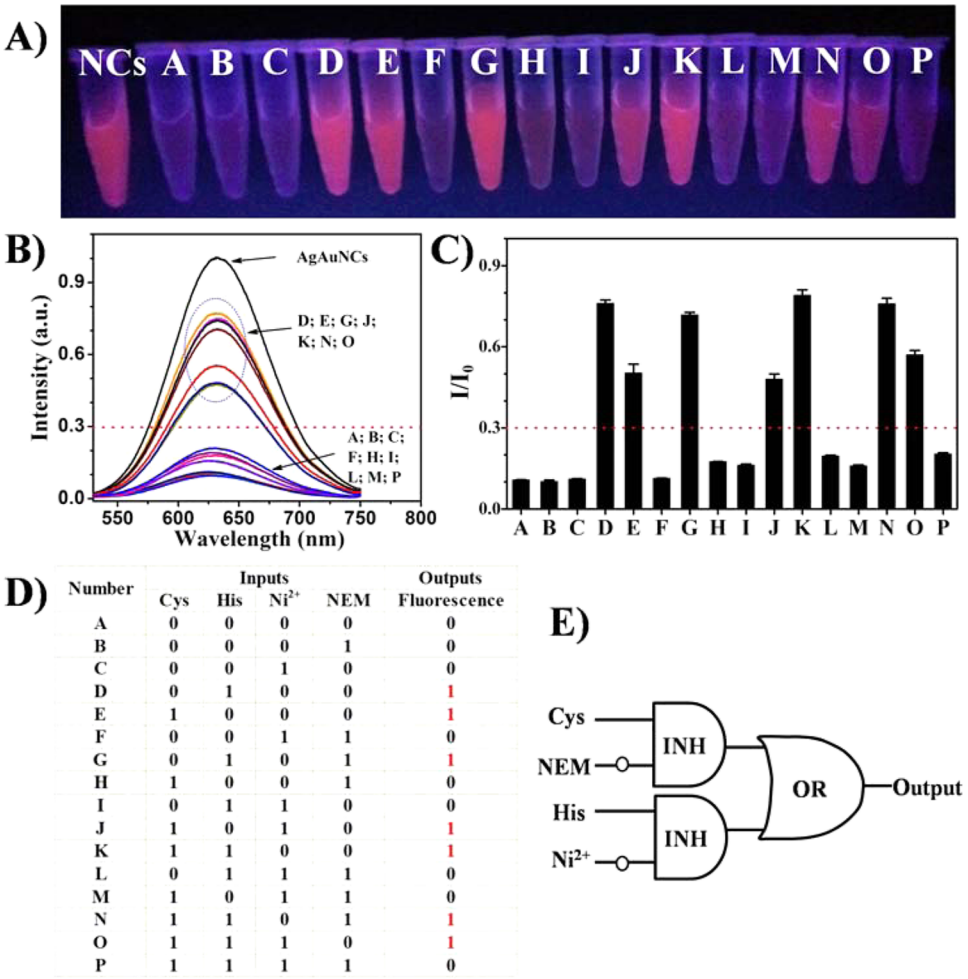

Number	Inputs				Outputs
	Cys	His	Ni^{2+}	NEM	Fluorescence
A	0	0	0	0	0
B	0	0	0	1	0
C	0	0	1	0	0
D	0	1	0	0	1
E	1	0	0	0	1
F	0	0	1	1	0
G	0	1	0	1	1
H	1	0	0	1	0
I	0	1	1	0	0
J	1	0	1	0	1
K	1	1	0	0	1
L	0	1	1	1	0
M	1	0	1	1	0
N	1	1	0	1	1
O	1	1	1	0	1
P	1	1	1	1	0

Figure 4. (A) Photographs of the AgAuNCs@11-MUA–Cu^{2+} ensemble for 16 input modes and the initial AgAuNCs as the control. (B) FL emission spectra of the AgAuNCs@11-MUA–Cu^{2+} ensemble for 16 input modes of the integrated logic gate and the initial AgAuNCs as the control. (C) FL intensity ratios (I/I_0 at 630 nm, where I and I_0 are the corresponding FL intensities for the 16 input modes and initial AgAuNCs). Measurements were performed by using 5 μM AgAuNCs in pH 7.4, 10 mM HEPES buffer. (D) Truth table and (E) logic scheme of the integrated logic gate of INH and OR. The output ratio below and above the threshold value of 0.3 defined as "0" and "1", respectively.

estimated to be 111 nM (S/N = 3). Besides, the tolerance experiments showed that the selective detection of Cys and His had been slightly affected by the coexistence of other amino acids (Figure S8 in the Supporting Information). It was noteworthy that Ni^{2+} not only showed an effective masking ability for His but also could trigger an obvious reduction in the fluorescence of the AgAuNCs@11-MUA (Figure 2A), especially when the concentration was above 10 μM (data not shown). Thus, our proposed bioassay has certain limits in Cys sensing in the presence of too many potentially interfering His molecules.

To evaluate the feasibility of our fluorescence turn-on detection method in real biological samples, we tested the potential interference effect of coexistent proteins in our bioassay. Taking two common proteins, human serum albumin and trypsin as examples, the existence of these control proteins (10 μg/mL) had little influence on the recognition behavior of the AgAuNCs–Cu^{2+} sensing ensemble (Figure S9 in the Supporting Information). Furthermore, the potential application of this proposed bioassay was illustrated through the further His analysis in diluted human urine samples.[34] As shown in Table S2 in the Supporting Information, the quantitative recoveries (94.4% to 110.3%) of spiked His have unambiguously demonstrated that the AgAuNCs–Cu^{2+} ensemble remained the His sensing ability, despite the interference from several complex components in human urine. Meanwhile, our detected concentrations of histidine (748 to 846 μM) in the human urine samples are consistent with its normal levels in human urine and that by other developed sensors.[34,42]

CONCLUSION

In summary, we first developed a straightforward one-pot strategy to synthesize fluorescent AgAuNCs@11-MUA, whose fluorescence was found to be selectively quenched by Cu^{2+} ions. By means of the reversible competitive coordination of Cu^{2+} between the certain amino acids and sole carboxyl group, the exquisite AgAuNCs@11-MUA–Cu^{2+} ensemble can be constructed as an integrated logic gate for specifically recognizing and differentiating His or Cys in the presence of Ni^{2+} or NEM. Moreover, our proposed fluorescence turn-on assay allows to sensitively detecting His in human urine samples with no need of any sample pretreatment procedures except dilution.

DOI: 10.1021/acsami.5b00434
ACS Appl. Mater. Interfaces 2015, 7, 6860–6866

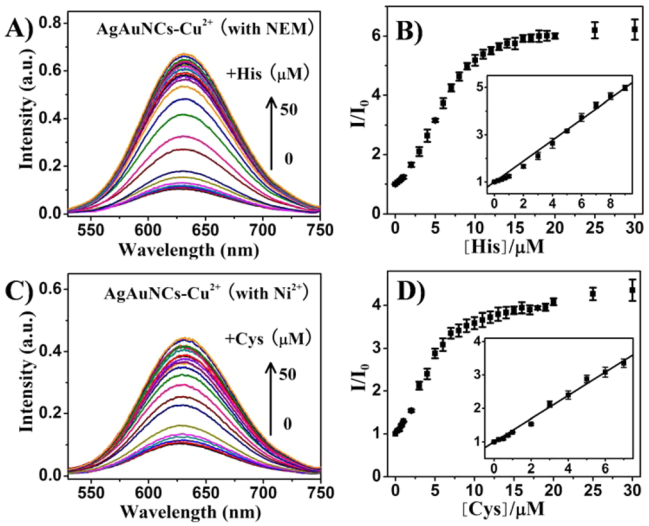

Figure 5. (A) FL emission spectra of the AgAuNCs@11-MUA–Cu^{2+} ensemble with 100 μM NEM in pH 7.4, 10 mM HEPES buffer upon addition of different concentrations of His increasing from 0 to 50 μM. (B) I/I_0 at 630 nm vs His concentration. Inset: plot of I/I_0 against the His ions concentrations. (C) FL emission spectra of the AgAuNCs–Cu^{2+} ensemble with 10 μM Ni^{2+} upon addition of different concentrations of Cys. (D) I/I_0 at 630 nm vs Cys concentration. Inset: plot of I/I_0 against the Cys ions concentrations.

■ ASSOCIATED CONTENT

Supporting Information

FL emission spectra and photographs of the AgAuNCs@11-MUA, AgAuNCs+Cu^{2+}, AgAuNCs+Cu^{2+}+His, and AgAuNCs +Cu^{2+}+Cys; UV–vis absorption, FL spectra, and photographs of AuNCs@11-MUA; the photostability of the AgAuNCs@11-MUA and AuNCs@11-MUA; XPS spectra of Ag 3d and S 2p for the AgAuNCs@11-MUA; TEM images and corresponding size distribution histograms of the AgAuNCs@11-MUA, AgAuNCs+Cu^{2+}, and AgAuNCs+Cu^{2+}+Cys; ICP-OES data and EDX spectra of the AgAuNCs@11-MUA; FL intensity ratios for the AgAuNCs by the addition of various amino acids; FL intensity ratios for the coexistence of other amino acids in the detection; the influence of control proteins on the recognition behavior; analytical results for His in the diluted human urine samples. This material is available free of charge via the Internet at http://pubs.acs.org.

■ AUTHOR INFORMATION

Corresponding Author

*X. Yang. E-mail: xryang@ciac.ac.cn. Fax: +86 431 85689278.

Notes

The authors declare no competing financial interest.

■ ACKNOWLEDGMENTS

This work was supported by the National Natural Science Foundation of China (No. 21435005, 21175124), and the Development Project of Science and Technology of Jilin Province (No. 20125090).

■ REFERENCES

(1) Zhou, Y.; Yoon, J. Recent Progress in Fluorescent and Colorimetric Chemosensors for Detection of Amino Acids. *Chem. Soc. Rev.* **2012**, *41*, 52–67.
(2) Luo, Z. T.; Zheng, K. Y.; Xie, J. P. Engineering Ultrasmall Water-Soluble Gold and Silver Nanoclusters for Biomedical Applications. *Chem. Commun.* **2014**, *50*, 5143–5155.
(3) Xu, J. J.; Zhao, W. W.; Song, S. P.; Fan, C. H.; Chen, H. Y. Functional Nanoprobes for Ultrasensitive Detection of Biomolecules: An Update. *Chem. Soc. Rev.* **2014**, *43*, 1601–1611.
(4) Peng, F.; Su, Y. Y.; Zhong, Y. L.; Fan, C. H.; Lee, S. T.; He, Y. Silicon Nanomaterials Platform for Bioimaging, Biosensing, and Cancer Therapy. *Acc. Chem. Res.* **2014**, *47*, 612–623.
(5) Huang, R. C.; Chiu, W. J.; Li, Y. J.; Huang, C. C. Detection of MicroRNA in Tumor Cells Using Exonuclease III and Graphene Oxide-Regulated Signal Amplification. *ACS Appl. Mater. Interfaces* **2014**, *6*, 21780–21787.
(6) Yuan, X.; Luo, Z. T.; Yu, Y.; Yao, Q. F.; Xie, J. P. Luminescent Noble Metal Nanoclusters as an Emerging Optical Probe for Sensor Development. *Chem.—Asian J.* **2013**, *8*, 858–871.
(7) Shang, L.; Dong, S. J.; Nienhaus, G. U. Ultra-small Fluorescent Metal Nanoclusters: Synthesis and Biological Applications. *Nano Today* **2011**, *6*, 401–418.
(8) Sun, J.; Jin, Y. D. Fluorescent Au Nanoclusters: Recent Progress and Sensing Applications. *J. Mater. Chem. C* **2014**, *2*, 8000–8011.
(9) Guo, W. W.; Yuan, J. P.; Dong, Q. Z.; Wang, E. K. Highly Sequence-Dependent Formation of Fluorescent Silver Nanoclusters in Hybridized DNA Duplexes for Single Nucleotide Mutation Identification. *J. Am. Chem. Soc.* **2010**, *132*, 932–934.
(10) Zhang, L. B.; Wang, E. K. Metal Nanoclusters: New Fluorescent Probes for Sensors and Bioimaging. *Nano Today* **2014**, *9*, 132–157.
(11) Yuan, Z. Q.; Chen, Y. C.; Li, H. W.; Chang, H. T. Fluorescent Silver Nanoclusters Stabilized by DNA Scaffolds. *Chem. Commun.* **2014**, *50*, 9800–9815.
(12) Chen, W. Y.; Lan, G. Y.; Chang, H. T. Use of Fluorescent DNA-Templated Gold/Silver Nanoclusters for the Detection of Sulfide Ions. *Anal. Chem.* **2011**, *83*, 9450–9455.
(13) Dou, X. Y.; Yuan, X.; Yu, Y.; Luo, Z. T.; Yao, Q. F.; Leong, D. T.; Xie, J. P. Lighting up Thiolated Au@Ag Nanoclusters via Aggregation-Induced Emission. *Nanoscale* **2014**, *6*, 157–161.
(14) Wang, S. X.; Meng, X. M.; Das, A.; Li, T.; Song, Y. B.; Cao, T. T.; Zhu, X. Y.; Zhu, M. Z.; Jin, R. C. A 200-Fold Quantum Yield Boost in the Photoluminescence of Silver Doped Ag_xAu_{25-X} Nanoclusters: The 13th Silver Atom Matters. *Angew. Chem., Int. Ed.* **2014**, *53*, 2376–2380.
(15) Zheng, J.; Zhou, C.; Yu, M. X.; Liu, J. B. Different Sized Luminescent Gold Nanoparticles. *Nanoscale* **2012**, *4*, 4073–4083.
(16) Shang, L.; Stockmar, F.; Azadfar, N.; Nienhaus, G. U. Intracellular Thermometry by Using Fluorescent Gold Nanoclusters. *Angew. Chem., Int. Ed.* **2013**, *52*, 11154–11157.
(17) Sun, J.; Yue, Y.; Wang, P.; He, H. L.; Jin, Y. D. Facile and Rapid Synthesis of Water-Soluble Fluorescent Gold Nanoclusters for Sensitive and Selective Detection of Ag^+. *J. Mater. Chem. C* **2013**, *1*, 908–913.
(18) Sun, J.; Zhang, J.; Jin, Y. D. 11-Mercaptoundecanoic Acid Directed One-Pot Synthesis of Water-Soluble Fluorescent Gold Nanoclusters and Their Use as Probes for Sensitive and Selective Detection of Cr^{3+} and Cr^{6+}. *J. Mater. Chem. C* **2013**, *1*, 138–143.
(19) Huang, C. C.; Yang, Z.; Lee, K. H.; Chang, H. T. Synthesis of Highly Fluorescent Gold Nanoparticles for Sensing Mercury(II). *Angew. Chem., Int. Ed.* **2007**, *46*, 6824–6828.
(20) Shang, L.; Yang, L. X.; Stockmar, F.; Popescu, R.; Trouillet, V.; Bruns, M.; Gerthsen, D.; Nienhaus, G. U. Microwave-Assisted Rapid Synthesis of Luminescent Gold Nanoclusters for Sensing Hg^{2+} in Living Cells Using Fluorescence Imaging. *Nanoscale* **2012**, *4*, 4155–4160.
(21) Roy, S.; Baral, A.; Banerjee, A. Tuning of Silver Cluster Emission from Blue to Red Using a Bio-active Peptide in Water. *ACS Appl. Mater. Interfaces* **2014**, *6*, 4050–4056.
(22) Fu, Y.; Li, H.; Hu, W.; Zhu, D. Fluorescence Probes for Thiol-Containing Amino Acids and Peptides in Aqueous Solution. *Chem. Commun.* **2005**, 3189–3191.

DOI: 10.1021/acsami.5b00434
ACS Appl. Mater. Interfaces 2015, 7, 6860–6866

(23) Reddy, G. U.; Agarwalla, H.; Taye, N.; Ghorai, S.; Chattopadhyay, S.; Das, A. A Novel Fluorescence Probe for Estimation of Cysteine/Histidine in Human Blood Plasma and Recognition of Endogenous Cysteine in Live HCT116 Cells. *Chem. Commun.* **2014**, *50*, 9899−9902.
(24) Sun, J.; Yang, F.; Zhao, D.; Yang, X. R. Highly Sensitive Real-Time Assay of Inorganic Pyrophosphatase Activity Based on the Fluorescent Gold Nanoclusters. *Anal. Chem.* **2014**, *86*, 7883−7889.
(25) Chen, Y.; Li, W. Y.; Wang, Y.; Yang, X. D.; Chen, J.; Jiang, Y. N.; Yu, C.; Lin, Q. Cysteine-Directed Fluorescent Gold Nanoclusters for the Sensing of Pyrophosphate and Alkaline Phosphatase. *J. Mater. Chem. C* **2014**, *2*, 4080−4085.
(26) Li, P. H.; Lin, J. Y.; Chen, C. T.; Ciou, W. R.; Chan, P. H.; Luo, L. Y.; Hsu, H. Y.; Diau, E. W. G.; Chen, Y. C. Using Gold Nanoclusters as Selective Luminescent Probes for Phosphate-Containing Metabolites. *Anal. Chem.* **2012**, *84*, 5484−5488.
(27) Kusakari, Y.; Nishikawa, S.; Ishiguro, S.; Tamai, M. Histidine-like Immunoreactivity in the Rat Retina. *Curr. Eye Res.* **1997**, *16*, 600−604.
(28) Watanabe, M.; Suliman, M. E.; Qureshi, A. R.; Garcia-Lopez, E.; Barany, P.; Heimburger, O.; Stenvinkel, P.; Lindholm, B. Consequences of Low Plasma Histidine in Chronic Kidney Disease Patients: Associations with Inflammation, Oxidative Stress, and Mortality. *Am. J. Clin. Nutr.* **2008**, *87*, 1860−1866.
(29) Gazit, V.; Ben-Abraham, R.; Coleman, R.; Weizman, A.; Katz, Y. Cysteine-Induced Hypoglycemic Brain Damage: An Alternative Mechanism to Excitotoxicity. *Amino Acids* **2004**, *26*, 163−168.
(30) Seshadri, S.; Beiser, A.; Selhub, J.; Jacques, P. F.; Rosenberg, I. H.; D'Agostino, R. B.; Wilson, P. W. F.; Wolf, P. A. Plasma Homocysteine as a Risk Factor for Dementia and Alzheimer's Disease. *N. Engl. J. Med.* **2002**, *346*, 476−483.
(31) Refsum, H.; Ueland, P. M.; Nygard, O.; Vollset, S. E. Homocysteine and Cardiovascular Disease. *Annu. Rev. Med.* **1998**, *49*, 31−62.
(32) Chen, G. N.; Wu, J. P.; Duan, J. P.; Chen, H. Q. A Study on Electrochemistry of Histidine and Its Metabolites Based on the Diazo Coupling Reaction. *Talanta* **1999**, *49*, 319−330.
(33) You, Q. H.; Lee, A. W. M.; Chan, W. H.; Zhu, X. M.; Leung, K. C. F. A Coumarin-based Fluorescent Probe for Recognition of Cu^{2+} and Fast Detection of Histidine in Hard-to-Transfect Cells by a Sensing Ensemble Approach. *Chem. Commun.* **2014**, *50*, 6207−6210.
(34) Wu, P.; Yan, X. P. Ni^{2+}-Modulated Homocysteine-Capped CdTe Quantum Dots as a Turn-on Photoluminescent Sensor for Detecting Histidine in Biological Fluids. *Biosens. Bioelectron.* **2010**, *26*, 485−490.
(35) Wei, M. J.; Yin, P.; Shen, Y. M.; Zhang, L. L.; Deng, J. H.; Xue, S. Y.; Li, H. T.; Guo, B.; Zhang, Y. Y.; Yao, S. Z. A New Turn-on Fluorescent Probe for Selective Detection of Glutathione and Cysteine in Living Cells. *Chem. Commun.* **2013**, *49*, 4640−4642.
(36) Huo, Z. Y.; Tsung, C. K.; Huang, W. Y.; Zhang, X. F.; Yang, P. D. Sub-Two Nanometer Single Crystal Au Nanowires. *Nano Lett.* **2008**, *8*, 2041−2044.
(37) Sun, J.; Wu, H. X.; Jin, Y. D. Synthesis of Thiolated Ag/Au Bimetallic Nanoclusters Exhibiting an Anti-Galvanic Reduction Mechanism and Composition-Dependent Fluorescence. *Nanoscale* **2014**, *6*, 5449−5457.
(38) Wang, B.; Gao, Y.; Li, H. W.; Hu, Z. P.; Wu, Y. Q. The Switch-on Luminescence Sensing of Histidine-rich Proteins in Solution: A Further Application of a Cu^{2+} Ligand. *Org. Biomol. Chem.* **2011**, *9*, 4032−4034.
(39) Liu, S. Y.; Shi, F. P.; Chen, L.; Su, X. G. Tyrosine-Functionalized $CuInS_2$ Quantum Dots as a Fluorescence Probe for the Determination of Biothiols, Histidine and Threonine. *Analyst* **2013**, *138*, 5819−5825.
(40) Szacilowski, K. Digital Information Processing in Molecular Systems. *Chem. Rev.* **2008**, *108*, 3481−3548.
(41) Pu, F.; Ju, E. G.; Ren, J. S.; Qu, X. G. Multiconfigurable Logic Gates Based on Fluorescence Switching in Adaptive Coordination Polymer Nanoparticles. *Adv. Mater.* **2014**, *26*, 1111−1117.
(42) Kovach, P. M.; Meyerhoff, M. E. Development and Application of a Histidine-Selective Biomembrane Electrode. *Anal. Chem.* **1982**, *54*, 217−220.

DOI: 10.1021/acsami.5b00434
ACS Appl. Mater. Interfaces 2015, 7, 6860−6866